

21-cm constraints on spinning primordial black holes

Junsong Cang,^{a,b} Yu Gao,^a Yin-Zhe Ma^{c,d}

^aKey Laboratory of Particle Astrophysics, Institute of High Energy Physics, Chinese Academy of Sciences, Beijing, 100049, China

^bSchool of Physical Sciences, University of Chinese Academy of Sciences, Beijing, 100049, China

^cSchool of Chemistry and Physics, University of KwaZulu-Natal, Westville Campus, Private Bag X54001, Durban, 4000, South Africa

^dNAOC–UKZN Computational Astrophysics Centre (NUCAC), University of KwaZulu-Natal, Durban, 4000, South Africa

E-mail: cangjs@ihep.ac.cn, gaoyu@ihep.ac.cn, ma@ukzn.ac.za

Abstract. Hawking radiation from primordial black holes (PBH) can ionize and heat up neutral gas during the cosmic dark ages, leaving imprints on the global 21-cm signal of neutral hydrogen. We use the global 21-cm signal to constrain the abundance of spinning PBHs in mass range of $[2 \times 10^{13}, 10^{18}]$ grams. We consider several extended PBH distribution models. Our results show that 21-cm can set the most stringent PBH bounds in our mass window. Compared with constraints set by *Planck* cosmic microwave background (CMB) data, 21-cm limits are more stringent by about two orders of magnitudes. PBHs with higher spin are typically more strongly constrained. Our 21-cm constraints for the monochromatic mass distribution rule out spinless PBHs with initial mass below 1.5×10^{17} g, whereas extreme Kerr PBHs with reduced initial spin of $a_0 = 0.999$ are excluded as the dominant dark matter component for masses below 6×10^{17} g. We also derived limits for the log-normal, power-law and critical collapse PBH mass distributions.

Contents

1	Introduction	1
2	Evaporating Black Holes	2
2.1	Particle Spectra	2
2.2	Evolving Mass and Spin Distributions	3
3	PBH imprints on IGM	7
3.1	Monochromatic mass distribution	8
3.2	Extended PBH distribution	9
4	21-cm limits	11
5	Summary	15

1 Introduction

The primordial black hole (PBH) is a type of hypothetical black holes (BH) that can be produced in the very early Universe due to the gravitational collapse of highly over-dense regions [1–4]. In addition to the connection with the theories of the early Universe, PBHs are considered as a dark matter (DM) component in numerous literature [5–11]. Compared with astrophysical BHs, PBHs can have masses ranging from 10^{-5} grams to beyond 10^{12} solar masses [7, 12]. These BHs can be detected through various techniques [7–23], ranging from gravitational wave [24] and lensing [25] to accretion [26–29].

PBHs lighter than 10^{18} grams emit Hawking radiation above keV, which can efficiently ionize and heat up the inter-galactic medium (IGM). The ionizing effect of PBH radiation increases number density of free electrons, which subsequently scatter off cosmic microwave background (CMB) photons [30], and PBHs can be constrained by the measurements of anisotropy spectra of CMB [31–36]. Also, IGM gas can be heated by PBH radiation, leading to a correction in the expected 21-cm signal from neutral hydrogen [37–39], which arises from hyperfine energy split between parallel and anti-parallel spin states of ground state hydrogen due to interaction of the magnetic moments between proton and electron [40]. Ignoring spatial inhomogeneity, the mean 21-cm brightness temperature in Λ CDM cosmology is given by [40, 41],

$$T_{21} \approx 27x_{\text{HI}} \left(\frac{\Omega_b h^2}{0.023} \right) \left(\frac{0.15}{\Omega_m h^2} \frac{1+z}{10} \right)^{1/2} \left(\frac{T_{\text{S}} - T_{\text{CMB}}}{T_{\text{S}}} \right) \text{mK} \quad (1.1)$$

where x_{HI} and T_{CMB} are neutral hydrogen fraction and CMB temperature. T_{S} is the spin temperature that characterizes the occupation numbers on the hydrogen atom’s split hyperfine states. After gas and the CMB decouple after around $z \sim 200$, T_{S} evolves separately from T_{CMB} . In particular in the early reionization era, T_{S} becomes tightly coupled to gas temperature T_{K} at around redshift $z = 20$ due to Wouthuysen-Field effect [40–44]. The PBH radiation’s potential heating effect on IGM gas temperature T_{K} would also raise T_{S} , causing a reduction in the expected 21-cm signal strength in comparison with that in vanilla Λ CDM.

The first detection of the 21-cm signal was claimed by the EDGES collaboration [45], which measured a T_{21} trough centered around redshift $z = 17$: $T_{21} = -500^{+200}_{-500}$ mK. Although the timing of this absorption profile is thought to be consistent with astrophysical expectations, the amplitude of the signal is deeper than the largest predictions by more than a factor of two [46]. Such deep absorption trough might be possible if excess radio background other than CMB were present [47–51], or if the gas temperature at this redshift were colder than 3.2 K [45], which can be achieved via the cooling effect of baryon-DM scattering [52–55]. In contrast, gas heating due to Hawking radiation raises T_K and the spin temperature T_S hence decreases the T_{21} amplitude, therefore Hawking radiation of PBH cannot explain the depth of EDGES signal. Nonetheless one can obtain very stringent limits on PBH abundance by requiring that the PBH heating does not wipe out the 21-cm signal [38, 39, 56].

Using the gas temperature upper limit inferred from a T_{21} upper bound consistent with EDGES result, in this work we constrain PBHs in the $[2 \times 10^{13}, 10^{18}]$ g mass window with several mass distributions. PBHs are normally assumed to have low spins [57–59], yet in some schemes it’s also possible for them to have high spins [9, 60–68]. Therefore in addition to the conventional Schwarzschild PBHs, we will also explore the parameter space of spinning Kerr PBHs. Although PBHs with initial mass below 10^{15} g would have evaporated away, they can still leave imprints on cosmic ionization and thermal history [33, 34, 37]. We also addressed several technical complications involving PBHs lighter than 10^{15} g. The first is that the emission of unstable standard particles, which decay or hadronize almost immediately after being emitted, will produce a cascade of secondary particles that carry on energy in the form of long-lived γ , e^\pm and ν [69]. Another complication is that the mass variation of PBHs lighter than 10^{15} g can no longer be ignored, which means that the PBH mass distribution would also evolve during the dark ages.

We discuss the particle spectra of Hawking evaporation and the evolution of mass and spin distribution in Sec. 2. Sec. 3 examines the impacts of PBHs on the evolution of cosmic gas temperature and ionization level. Our results are presented in Sec. 4 and we conclude in Sec. 5. We assume the spatially-flat Λ CDM cosmology with the relevant parameters set by *Planck* 2018 results [70]: $h = 0.6766$, $\Omega_b h^2 = 0.02242$, $\Omega_c h^2 = 0.11933$, $\tau = 0.0561$, $\log(10^{10} A_s) = 3.047$, $n_s = 0.9665$.

2 Evaporating Black Holes

2.1 Particle Spectra

The temperature of Hawking radiation emitted by a Kerr black hole is [9, 71–74]

$$T_{\text{PBH}} = \frac{1}{4\pi M} \frac{\sqrt{1-a^2}}{1+\sqrt{1-a^2}} = 2.12 \times \frac{10^3 \text{g}}{M} \frac{\sqrt{1-a^2}}{1+\sqrt{1-a^2}} \text{GeV}, \quad (2.1)$$

where M is PBH mass, a is the reduced dimensionless spin parameter, defined as

$$a \equiv J/M^2 \in [0, 1], \quad (2.2)$$

and J is the angular momentum of the BH. The primary particle emission spectra of a BH is given by [69, 72–75]

$$\left[\frac{dN^\alpha}{dE dt} \right]_{\text{pri}} = \frac{1}{2\pi} \sum_{\text{dof}} \frac{\Gamma^\alpha}{e^{E'/T_{\text{PBH}}} - (-1)^{2s}}, \quad E' = E - \frac{m}{2M} \frac{a}{1+\sqrt{1-a^2}}, \quad (2.3)$$

here the subscript ‘pri’ denotes primary emission, α labels particle species, s is the spin of the particle, Γ^α is the greybody factor [69, 72–74]. The sum is over the total multiplicity of the particle as well as the angular momentum l and its z -component $m \in \{-l, \dots, l\}$.

The prompt particle spectra ($dN^\alpha/dEdt$) for stable particle species, which contains both primary and secondary emissions, is computed as (see also Ref. [73, 74]),

$$\left[\frac{dN^\alpha}{dEdt}\right](M, a, E) = \left[\frac{dN^\alpha}{dEdt}\right]_{\text{pri}}(M, a, E) + \frac{1}{2} \sum_{\alpha'} \int dE' \frac{dN^\alpha}{dE}(E, E') \left[\frac{dN^{\alpha'}}{dEdt}\right]_{\text{pri}}(M, a, E'), \quad (2.4)$$

where dN^α/dE is the energy spectra of α produced by decay/hadronization of a pair of unstable α' particles with center of mass energy of $2E'$, α' runs through all directly emitted standard model particles except for (e^\pm, γ, ν) .

We use the **BlackHawk** package [73, 74] to calculate the particle spectra ($dN^\alpha/dEdt$) and evolution of PBH mass M and spin a . Due to Hawking radiation, a PBH will lose its mass at a rate given by [72–74, 76],

$$\frac{dM}{dt} = -\frac{f(M)}{M^2}. \quad (2.5)$$

Here f is the Page factor [72],

$$f \equiv -M^2 \frac{dM}{dt} = M^2 \sum_{\alpha} \int_0^\infty dE E \left[\frac{dN^\alpha}{dEdt}\right]_{\text{pri}}, \quad (2.6)$$

and the sum is over all standard model particle species. For the Schwarzschild PBHs ($a = 0$) in particular, the Page factor can be written as [33, 77]

$$f = 5.34 \times 10^{25} \mathcal{F} \text{ g}^3/\text{s}, \quad (2.7)$$

$$\mathcal{F} = \sum_{\alpha} g^\alpha \omega^\alpha \exp(-M/M^\alpha) \in [1, 16.4]. \quad (2.8)$$

Here g^α is the internal degrees of freedom of particle α , ω^α and M^α are relativistic emission fraction and characteristic BH mass for each particle species, whose values have been tabulated in Refs. [33]. In general, smaller PBHs evaporates more violently than heavier ones, a Schwarzschild PBH with $M < 7.9 \times 10^{14} \text{ g}$ would have completely evaporated before the present day. In $[2 \times 10^{13}, 10^{18}] \text{ g}$ mass range considered here, such mass loss can cause non-negligible modification to BH mass distributions and energy injection history.

2.2 Evolving Mass and Spin Distributions

When mass loss and spin-down is significant during the age of the Universe, the PBH mass and spin evolution with redshift need to be taken care of properly. Ignoring mergers, the number of PBHs are conserved prior to their final complete evaporation. The mass distribution of PBHs can be described through their mass density ρ and number density n at comoving frame,

$$\Psi(M, t) \equiv \frac{1}{\rho_0} \frac{d\rho}{dM}, \quad (2.9)$$

$$\Phi(M, t) \equiv \frac{1}{n_0} \frac{dn}{dM}, \quad (2.10)$$

where ρ_0 and n_0 are initial *comoving* BH mass and number density at some early time $t = t_0$,

$$\rho_0 = f_{\text{PBH}} \rho_c, \quad (2.11)$$

here ρ_c is the comoving cold dark matter density, $f_{\text{PBH}} \equiv \rho_0/\rho_c$ is the initial fraction of dark matter made of PBH.

We assume that $t_0 \ll \tau_{\text{min}}$, where $\tau_{\text{min}} \sim 5 \times 10^4$ yrs is the lifetime of the most short-lived PBH considered here. Both $\Psi(M, t)$ and $\Phi(M, t)$ are normalized to unity at t_0 , however they do not stay normalized if a fraction of PBH evaporate away at $t > t_0$. One can obtain $\Phi(M, t)$ from $\Psi(M, t)$ (and vice versa) by

$$\Delta n = n_0 \int_{M'}^{M''} dM \Phi(M, t) = \rho_0 \int_{M'}^{M''} dM \frac{\Psi(M, t)}{M}, \quad (2.12)$$

which gives,

$$\Phi = C \frac{\Psi}{M}, \quad C^{-1} = \int_0^\infty dM \frac{\Psi(M, t_0)}{M}, \quad (2.13)$$

with the normalization factor C set by the normalization conditions for Ψ and Φ at t_0 ,

$$1 = \int_0^\infty dM \Phi(M, t_0) = C \int_0^\infty dM \frac{\Psi(M, t_0)}{M}. \quad (2.14)$$

Since Ψ and Φ are essentially equivalent, hereafter we will use Ψ to describe PBH mass distribution. In the simplified monochromatic approximation, in which all PBHs have the same mass,

$$\Psi(M, t_0) = \delta_D(M - M_0), \quad (2.15)$$

where M_0 indicates the initial mass of BH at t_0 . This monochromatic model is a convenient approximation, and many PBH formation theories tend to favor extended distributions [78–84], therefore we also consider the following three theoretically motivated extended mass distribution scenarios:

- Log-normal model [78–80]

$$\Psi(M, t_0) = \frac{1}{\sqrt{2\pi}\sigma M} \exp\left(-\frac{(\log[M/M_c])^2}{2\sigma^2}\right), \quad (2.16)$$

- Critical Collapse model [79, 81, 82]

$$\Psi(M, t_0) = \frac{3.2}{M_c} \left(\frac{M}{M_c}\right)^{2.85} \exp\left[-\left(\frac{M}{M_c}\right)^{2.85}\right], \quad (2.17)$$

- Power-law model [79]

$$\Psi(M, t_0) = \frac{\gamma}{M_{\text{max}}^\gamma - M_{\text{min}}^\gamma} M^{\gamma-1}, \quad M \in [M_{\text{min}}, M_{\text{max}}]. \quad (2.18)$$

Here the power-law index γ is related to the equation of state parameter ω during PBH formation by $\gamma = -2\omega/(1 + \omega)$, therefore for post-inflation epochs $0 < |\gamma| \leq 1$. PBH

production at matter dominated era with $\gamma = 0$ requires special treatment (e.g. see [85]) and is not considered here.

Note that Eqs. (2.16) - (2.18) are all given at $t = t_0$, their evolved forms can be tracked by imposing that the BH numbers are conserved (until before the smallest BH evaporate away),

$$\Delta n = \rho_0 \int_{M'_0}^{M''_0} dM_0 \frac{\Psi(M_0, t_0)}{M_0} = \rho_0 \int_{M'}^{M''} dM \frac{\Psi(M, t)}{M}, \quad M' > 0 \quad (2.19)$$

which gives

$$\Psi(M, t) = \Psi[M_0, t_0] \times \frac{dM_0}{dM} \frac{M}{M_0}, \quad (2.20)$$

where $M_0(M, t)$ indicates the initial mass of a BH with mass M at t . Analogously one can start from

$$\Delta n = n_0 \int_{M'_0}^{M''_0} dM_0 \cdot \Phi(M_0, t_0) = n_0 \int_{M'}^{M''} dM \cdot \Phi(M, t), \quad M' > 0, \quad (2.21)$$

to show that

$$\Phi(M, t) = \Phi[M_0, t_0] \times \frac{dM_0}{dM}. \quad (2.22)$$

In addition to Hawking radiation, there could also be other physical processes that can change the mass and spin of PBHs, most notably BH mergers [86–89] and accretion [90]. It's possible that PBH spin can also have extended distributions [68, 73, 74, 86, 87, 90–93], but these complicated scenarios are beyond the scope of this paper, therefore we will adopt the same strategy as Refs. [9–11] and restrict our discussions to PBHs born with the same initial spin.

Equation (2.19) is equivalent to the requirement that Hawking radiation does not change mass ordering of PBHs, such that any BH initially heavier than M'_0 will always be present provided that M'_0 does not vanish at t . This is true for Schwarzschild PBHs, for which heavier PBHs always evaporate at a slower rate. For Kerr PBHs however, it's more complicated as a BH may lose energy faster than a less massive one of lower spin. In practice, one may always bin the PBH spin distribution and sum up the evolved contributions from each bin later. Thus we can consider BHs of some fixed initial spin a_0 . For each fixed initial spin, we numerically simulated the mass evolution M_0 values in the $[2 \times 10^{13}, 10^{18}]$ g range, and we find that the ordering of evolved mass is maintained in the redshift range of interest ($z \in [11, 2.7 \times 10^3]$). Therefore Eq. (2.20) also holds for PBHs with a common initial spin, and we will use it to study the evolved distribution for both Schwarzschild PBHs and Kerr BHs with a certain initial spin.

Hawking radiation also cause a BH to gradually lose its spin at a rate given by (see also [72–74, 76]),

$$\frac{da}{dt} = a \frac{2f - g}{M^3}, \quad (2.23)$$

$$g \equiv -\frac{M}{a} \frac{dJ}{dt} = \frac{M}{a} \sum_{\alpha} \int_0^{\infty} dE \, m \left[\frac{dN^{\alpha}}{dE dt} \right]_{\text{pri}}. \quad (2.24)$$

An example of mass and spin evolution as computed by **BlackHAWK** is shown in the left panel of Fig. 1. Typically smaller PBHs also lose their spin faster than heavier ones, therefore for PBHs with the same initial spin, as Hawking radiation progresses, PBH mass and spin

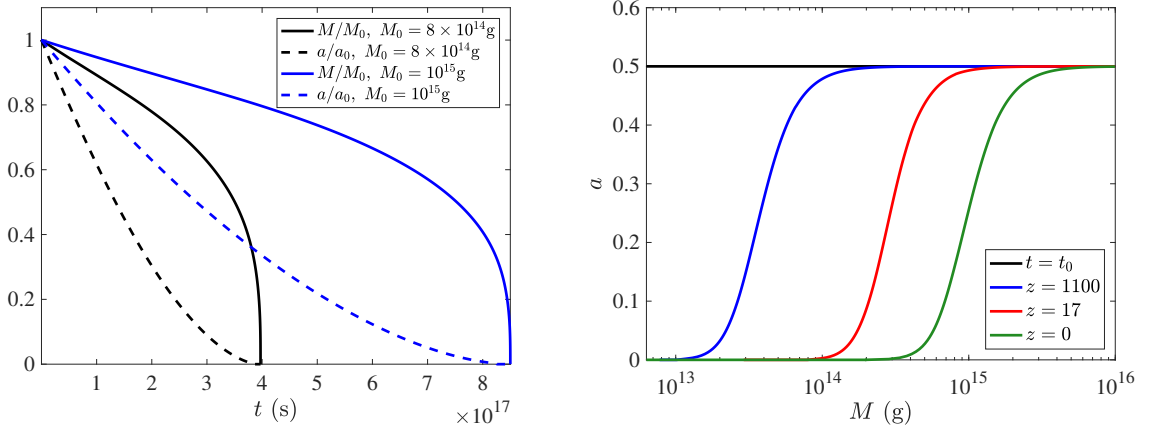


Figure 1. *Left:* Mass (solid) and spin (dashed) evolution of two PBHs with initial masses of 8×10^{14} g (black) and 10^{15} g (blue). *Right:* Evolved spin for survived PBH masses at redshifts of 1100 (blue), 17 (red) and 0 (green). All PBHs are assumed to have same initial spin of $a_0 = 0.5$ in both panels.

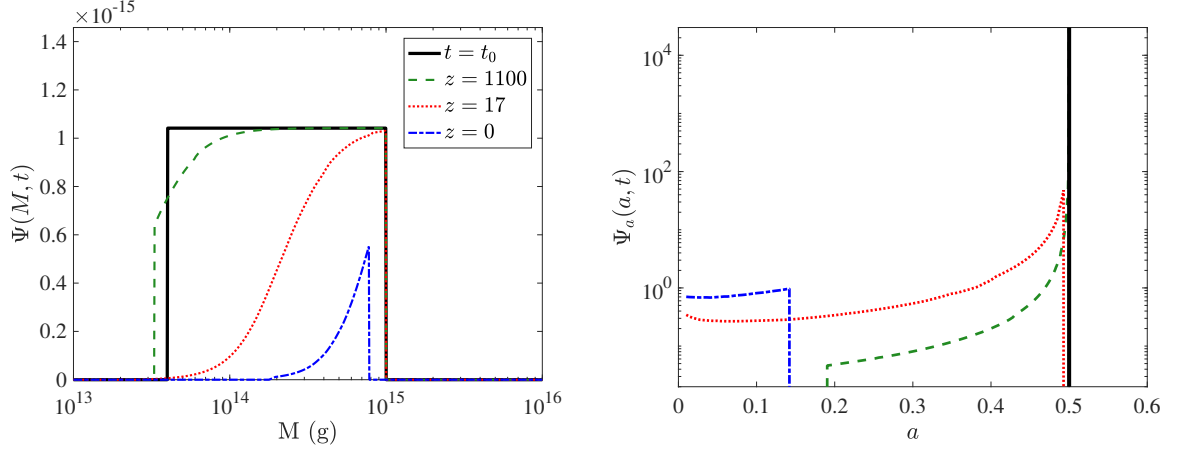


Figure 2. Evolution of a uniform box-like power-law mass distribution (*left*) with $\gamma = 1$, $M_{\min} = 4 \times 10^{13}$ g, $M_{\max} = 10^{15}$ g, the corresponding spin distributions are shown in the *right* panel. The black solid, green dashed, red dotted, blue dot-dashed lines correspond to redshifts of ∞ ($t = t_0$), 1100 (recombination), 17 (EDGES redshift) and 0 (present) respectively. All PBHs are assumed to have the same initial spin of $a_0 = 0.5$, legend applies to both panels.

evolution will become correlated. The right panel in Fig. 1 shows the evolution of spin-mass relation for an initial spin of $a_0 = 0.5$. For extended mass distributions, this correlation will cause PBH spins to spread from a monochromatic initial distribution to an extended distribution, which itself is related to the mass distribution simply by,

$$\Psi_a(a, t) \equiv \frac{1}{\rho_0} \frac{d\rho}{da} = \Psi[M(a), t] \frac{dM}{da}, \quad (2.25)$$

where $\Psi_a(a, t)$ is the spin distribution. The monochromatic initial spin distribution as considered here is given by

$$\Psi_a(a, t_0) = \delta_D(a - a_0), \quad (2.26)$$

In Fig. 2 we show the evolution of a uniform box-like mass distribution and the corresponding spin distribution. The black solid lines show the initial distributions, and their evolved forms given by Eqs. (2.20) and (2.25) are shown in green dashed, red dotted and blue dot-dashed lines. Since the fractional mass and spin loss of even the smallest PBH considered in the figure only becomes noticeable after $z = 1100$, the evolution in $\Psi(M, t)$ and $\Psi_a(a, t)$ remains negligible until the recombination epoch, and the numerical integration of the green lines in both panels consistently reveals that $\rho/\rho_0 = \int da \Psi_a(a, t) = \int dM \Psi(M, t) > 0.99$, which suggests that at $z = 1100$, more than 99% of the initial PBH mass density ρ_0 remain untouched by evaporation.

3 PBH imprints on IGM

Radiation from evaporating PBHs propagate through the Universe and gradually damp their energy into the IGM through occasional collisions with the intergalactic gas. Consequent impact on the CMB and 21-cm mainly occurs via enhanced ionization fraction and gas temperature. In this section, we will calculate the energy injection rate due to PBH radiation for a few characteristic PBH mass distributions, and their energy deposit rate into the IGM. Such energy deposit sources will modify the evolution of IGM temperature T_K and ionization level $x_e \equiv n_e/n_H$ during the cosmic dark age.

In the scope of this paper, energy released by evaporating PBHs is absorbed by the IGM mainly through three deposition channels: IGM heating (Heat), hydrogen ionization (HIon) and excitation ($\text{Ly}\alpha$). In presence of these extra energy deposition processes, the modification to the standard evolution equations for T_K and x_e take the form [31, 94–96],

$$\frac{dT_K}{dt} = \left[\frac{dT_K}{dt} \right]_0 + \frac{2}{3n_H(1 + f_{\text{He}} + x_e)} \left[\frac{dE}{dV dt} \right]_{\text{dep, Heat}}, \quad (3.1)$$

$$\frac{dx_e}{dt} = \left[\frac{dx_e}{dt} \right]_0 + \frac{1}{n_H(z)E_i} \left[\frac{dE}{dV dt} \right]_{\text{dep, HIon}} + \frac{1 - C}{n_H(z)E_\alpha} \left[\frac{dE}{dV dt} \right]_{\text{dep, Ly}\alpha}. \quad (3.2)$$

Here $E_i = 13.6$ eV and $E_\alpha = 10.2$ eV. The first term with subscript 0 denotes for the standard evolution equation (see Refs. [97, 98]) without PBH radiation injection. $[dE/dV dt]_{\text{dep, c}}$ is the energy deposition rate per unit volume (hereafter dubbed deposition rate for simplicity) through absorption channel $c \in [\text{HIon}, \text{Ly}\alpha, \text{Heat}]$. f_{He} is the helium fraction by number of nuclei, C is Pebble’s C factor [94, 95, 98] which describes the probability for an excited $n = 2$ hydrogen atom to transit back to ground state before being ionized. Eq. 3.1 and 3.2 are implemented in our customized HyRec package to compute the T_K and x_e evolution with PBH radiation injection contributions.

Since e^\pm and γ make up the majority of emitted stable particles with sufficient electromagnetic interaction with the IGM, one can calculate the energy deposition rate by tracking the IGM interaction of radiated e^\pm and γ , whose energy deposition processes at redshift z can be described by a transfer function $\mathcal{T}_c^\alpha(z, E, z')$ [99] from the radiation energy injected at an earlier redshift z' . For a particle $\alpha \in [\gamma, e^\pm]$ injected at z' with energy E , $\mathcal{T}_c^\alpha(z, E, z')$ gives the fraction of E absorbed into channel c during unit $-\log(1+z)$ interval. For a generic

particle injection history, the relevant deposition rate is given by (see also [99, 100]),

$$\begin{aligned} \left[\frac{dE}{dV dt} \right]_{\text{dep,c}}(z) &= \frac{dx}{dt} \int dt' \sum_{\alpha=\gamma,e^\pm} \left[\int dE E \mathcal{T}_c^\alpha(z, E, z') \mathcal{I}^\alpha(E, z') \frac{dV'}{dV} \right] \\ &= (1+z)^3 H(z) \int \frac{dz'}{(1+z')^4 H(z')} \sum_{\alpha=\gamma,e^\pm} \left[\int dE E \mathcal{T}_c^\alpha(z, E, z') \mathcal{I}^\alpha(E, z') \right], \end{aligned} \quad (3.3)$$

where $x \equiv -\log(1+z)$, and in the second line we used relations $dt' = dx'/H(z')$, $dV \propto (1+z)^{-3}$ and $dV' \propto (1+z')^{-3}$. \mathcal{I}^α is the differential particle injection rate per unit volume,

$$\mathcal{I}^\alpha \equiv \frac{dN^\alpha}{dE dV dt}, \quad (3.4)$$

we will elaborate on this term in next two subsections.

3.1 Monochromatic mass distribution

Assuming a monochromatic PBH mass distribution $\delta(M - M_0)$, and a given initial spin a_0 , the particle injection history \mathcal{I}^α in Eq. (3.3) takes the form,

$$\mathcal{I}^{\alpha,\delta}(M_0, a_0, E, z) = \left[\frac{dN^\alpha}{dE dt} \right] (M, a, E) \cdot n_{\text{PBH}} \times \Theta[\tau_{\text{PBH}}(M_0, a_0) - t] \quad (3.5)$$

where $dN^\alpha/dE dt$ is computed through Eq. (2.4), superscript δ indicates monochromatic distribution, M is the mass of M_0 at redshift z , τ_{PBH} is the lifetime of M_0 , t is the age of the Universe at redshift z , Θ is the Heaviside step function which enforces $\mathcal{I}^{\alpha,\delta}$ to vanish once M_0 reaches its' end of life. n_{PBH} is PBH number density,

$$n_{\text{PBH}}(z) = f_{\text{PBH}} \frac{\Omega_c \rho_{\text{cr}} (1+z)^3}{M_0}. \quad (3.6)$$

where ρ_{cr} is the current critical density of the Universe. Inserting Eqs. (3.5,3.6) into Eq. (3.3) gives the deposition rate for monochromatic PBHs,

$$\begin{aligned} \left[\frac{dE}{dV dt} \right]_{\text{dep,c}}^\delta(M_0, a_0, z) &= \frac{f_{\text{PBH}} \Omega_c \rho_{\text{cr}} H(z) (1+z)^3}{M_0} \int \frac{dz'}{(1+z') H(z')} \\ &\times \sum_{\alpha=\gamma,e^\pm} \left[\int dE E \mathcal{T}_c^\alpha(z, E, z') \left[\frac{dN^\alpha}{dE dt} \right]' \Theta(\tau_{\text{PBH}} - t') \right], \end{aligned} \quad (3.7)$$

here t' is the age of the Universe at redshift z' , $[dN^\alpha/dE dt]'$ is the $dN^\alpha/dE dt$ spectra at z' , when the PBH mass and spin would have evolved from $[M_0, a_0]$ to $[M, a]$. The superscript δ denotes for the monochromatic distribution.

The energy injection rate per unit physical volume (dubbed injection rate hereafter) from monochromatic PBHs can be written as,

$$\left[\frac{dE}{dV dt} \right]_{\text{inj}}^\delta(M_0, a_0, z) = \frac{dE}{dt} \cdot n_{\text{PBH}} \Theta[\tau_{\text{PBH}} - t]. \quad (3.8)$$

here dE/dt indicates the power of Hawking radiation, which is equal to $-dM/dt$ if $a_0 = 0$. Eq. (3.8) has a simple analytic form for Schwarzschild PBHs with $M_0 \geq 10^{17}$ g, for which the factor \mathcal{F} in Eq. (2.8) is normalized to unity [33, 77] and therefore

$$\frac{dE}{dt} = -\frac{dM}{dt} = 5.34 \times 10^{25} \left(\frac{g}{M}\right)^2 \text{ g/s.} \quad (3.9)$$

where we have used Eqs. (2.5, 2.7). For $M_0 \geq 10^{17}$ g, the fractional mass loss $\Delta M/M_0$ remains negligible across the entire history of the Universe, thus one can safely set $M = M_0$ in Eq. (3.9) and ignore the step function $\Theta[\tau_{\text{PBH}} - t]$ in Eq. (3.8), therefore inserting Eq. (3.9) into Eq. (3.8) gives,

$$\left[\frac{dE}{dV dt} \right]_{\text{inj}}' = 5.34 \times 10^{25} (M_0/\text{g})^{-3} f_{\text{PBH}} \Omega_c \rho_{\text{cr}} (1+z)^3 \text{ s}^{-1}. \quad (3.10)$$

Although $[dE/dV dt]_{\text{inj}}'$ does not accurately reproduce $[dE/dV dt]_{\text{inj}}^\delta$ if $M_0 < 10^{17}$ g or $a_0 > 0$, it is convenient to relate it to the actual deposition rate through an effective deposition efficiency, defined as,

$$f_c(z) \equiv \left[\frac{dE}{dV dt} \right]_{\text{dep,c}}^\delta / \left[\frac{dE}{dV dt} \right]_{\text{inj}}', \quad (3.11)$$

f_c can be pre-computed numerically, such that deposition rate at any given redshift can be recovered through,

$$\left[\frac{dE}{dV dt} \right]_{\text{dep,c}}^\delta(z) = f_c(z) \times \left[\frac{dE}{dV dt} \right]_{\text{inj}}'. \quad (3.12)$$

Using Eqs. (3.7, 3.10, 3.11), after re-arranging terms, f_c reads

$$\begin{aligned} f_c(M_0, a_0, z) &= \frac{H(z)}{5.34 \times 10^{25}} \left(\frac{M_0}{\text{g}}\right)^2 \int \frac{dz'}{(1+z')H(z')} \\ &\times \sum_{\alpha=\gamma, e^\pm} \int dE E \mathcal{T}_c^\alpha(z, E, z') \left[\frac{dN^\alpha}{dE dt} \right]' \Theta(\tau_{\text{PBH}} - t') \text{ s} \cdot \text{g}^{-1}. \end{aligned} \quad (3.13)$$

Fig. 3 shows f_c for all deposition channels and a_0 values considered in this work. Since one must perform integration in Eqs. (3.3) and (3.13) over all injection redshifts prior to z , f_c at any given redshift receives contribution from particle injected at earlier redshifts, therefore deposition rate at a certain redshift can be nonzero even when the injection source, i.e PBH, has already vanished. Another interesting feature about Fig. 3 is the sudden increase in f_c when a PBH reaches the end of its lifetime, caused by the surge of energy injection rate during PBH explosion.

3.2 Extended PBH distribution

In analogy to Eq. (3.5), for PBHs with extended distribution, the differential form of the particle injection history \mathcal{I}^α is given by

$$d\mathcal{I}^\alpha = \left[\frac{dN^\alpha}{dE dt} \right] (M) dn_{\text{PBH}} \quad (3.14)$$

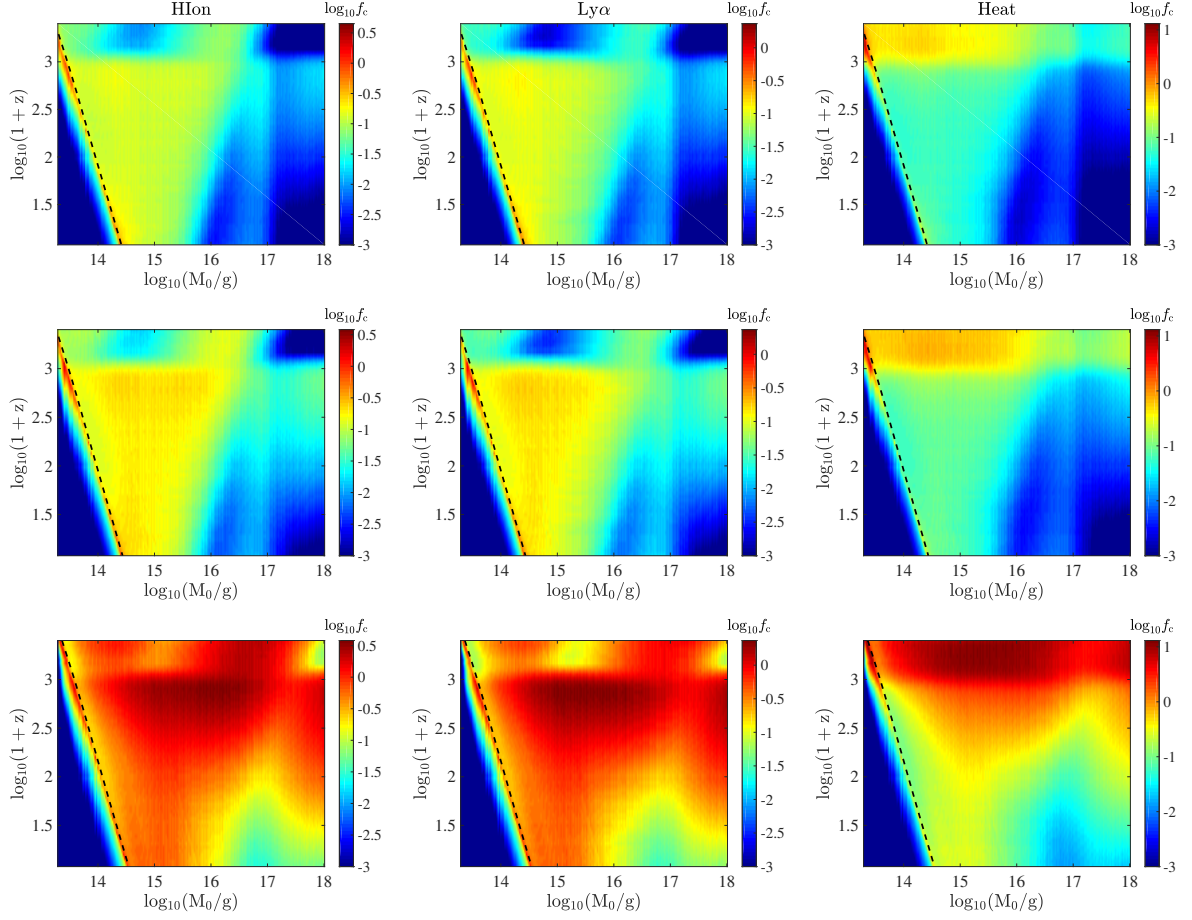


Figure 3. Effective deposition efficiency f_c defined in Eq. (3.11) for monochromatic PBHs. The deposition channels are hydrogen ionization (left), hydrogen excitation (middle) and heating (right), the top, middle and bottom rows correspond to a_0 values of 0, 0.5 and 0.999 respectively. Redshifts when the PBH reaches its' end of life are indicated by black dashed lines. f_c values lower than 10^{-3} have been set to 10^{-3} here for illustrative purpose (dark blue regions).

here dn_{PBH} is the number density of PBHs in mass range $[M, M + dM]$,

$$\begin{aligned}
 dn_{\text{PBH}} &= (1+z)^3 \frac{d\rho}{M} \\
 &= f_{\text{PBH}} \Omega_c \rho_{\text{cr}} (1+z)^3 \Psi(M, t) \frac{dM}{M} \\
 &= f_{\text{PBH}} \Omega_c \rho_{\text{cr}} (1+z)^3 \Psi(M_0, t_0) \frac{dM_0}{M_0}
 \end{aligned} \tag{3.15}$$

where we used Eqs. (2.9, 2.11) in the second line and Eq. (2.20) in the third line. Inserting this equation into Eq. (3.14) and integrating over all survived M_0 values gives,

$$\mathcal{I}^\alpha(z) = f_{\text{PBH}} \Omega_c \rho_{\text{cr}} (1+z)^3 \int_{M_0^{\min}(z)}^{\infty} \frac{dM_0}{M_0} \left[\frac{dN^\alpha}{dEdt} \right] (M) \Psi(M_0, t_0) \tag{3.16}$$

$M_0^{\min}(z)$ is the mass of PBH whose lifetime τ_{PBH} equals $t(z)$, or equivalently the smallest initial PBH mass that can survive to redshift z . Comparing this equation with Eq. (3.5), one

finds that

$$\mathcal{I}^\alpha(z) = \int_0^\infty dM_0 \mathcal{I}^{\alpha,\delta}(M_0, z) \Psi(M_0, t_0). \quad (3.17)$$

We have moved lower limit of M_0 integration from $M_0^{\min}(z)$ to 0 because $\mathcal{I}^{\alpha,\delta}(M_0, z)$ given by Eq. (3.5) automatically vanishes once M_0 reaches its end of life, therefore M_0 integration from 0 to $M_0^{\min}(z)$ does not change the results of Eq. (3.17). Inserting Eq. (3.17) into Eq. (3.3) gives the deposition rate for extended PBH distribution,

$$\begin{aligned} \left[\frac{dE}{dV dt} \right]_{\text{dep,c}}(z) &= (1+z)^3 H(z) \int \frac{dz'}{(1+z')^4 H(z')} \\ &\times \sum_{\alpha=\gamma, e^\pm} \int dE E \mathcal{T}_c^\alpha(z, E, z') \left[\int_0^\infty dM_0 \mathcal{I}^{\alpha,\delta}(M_0, z') \Psi(M_0, t_0) \right] \\ &= \int_0^\infty dM_0 \Psi(M_0, t_0) (1+z)^3 H(z) \\ &\times \int \frac{dz'}{(1+z')^4 H(z')} \sum_{\alpha=\gamma, e^\pm} \left[\int dE E \mathcal{T}_c^\alpha(z, E, z') \mathcal{I}^{\alpha,\delta}(E, z') \right], \end{aligned} \quad (3.18)$$

which can be simplified as an integration over deposition rate for a monochromatic distribution at M_0 ,

$$\left[\frac{dE}{dV dt} \right]_{\text{dep,c}}(z) = \int_{2 \times 10^{13} \text{g}}^{10^{18} \text{g}} dM_0 \Psi(M_0, t_0) \left[\frac{dE}{dV dt} \right]_{\text{dep,c}}^\delta(M_0, z). \quad (3.19)$$

where the integrated M_0 range has been set to the mass window considered in this work. Similarly one can also show that injection rate for extended distribution follows an analogous relation,

$$\left[\frac{dE}{dV dt} \right]_{\text{inj}}(z) = \int_0^\infty dM_0 \Psi(M_0, t_0) \left[\frac{dE}{dV dt} \right]_{\text{inj}}^\delta(M_0, z). \quad (3.20)$$

For typical extended mass distributions, we will consider log-normal, critical collapse and power-law scenarios as in Eqs. 2.16-2.18. The IGM temperature rise and T_{21} correction at early reionization epoch are numerically evaluated and compared to experimentally measured upper limits. Corresponding limits on the PBH injection rate are given in the next section.

4 21-cm limits

IGM temperature and ionization evolutions, after accounting for PBH heating/ionization effects as in Eqs. (3.1,3.2), are numerically computed by modified HyRec package [97]. IGM heating's impact on 21-cm signal reveals after Wouthuysen-Field effect takes place, where the hydrogen spin temperature T_S becomes bound to gas temperature T_K . PBH heating increases gas temperature T_K which is typically closely coupled to T_S at redshift $z = 17$ [40, 41], and in turn damps the amplitude of T_{21} signal observed by EDGES. Here we derive our 21-cm upper bounds on f_{PBH} by imposing that PBH does not over-heats the IGM gas, or equivalently raises T_{21} beyond -150 mK,

$$T_{21} < -150 \text{mK, at } z = 17. \quad (4.1)$$

This choice is noticeably higher than both the EDGES 99% C.L. upper limit of -300 mK, and the standard Λ CDM lower limit of -210 mK [54, 101]. Generally T_S is coupled to both

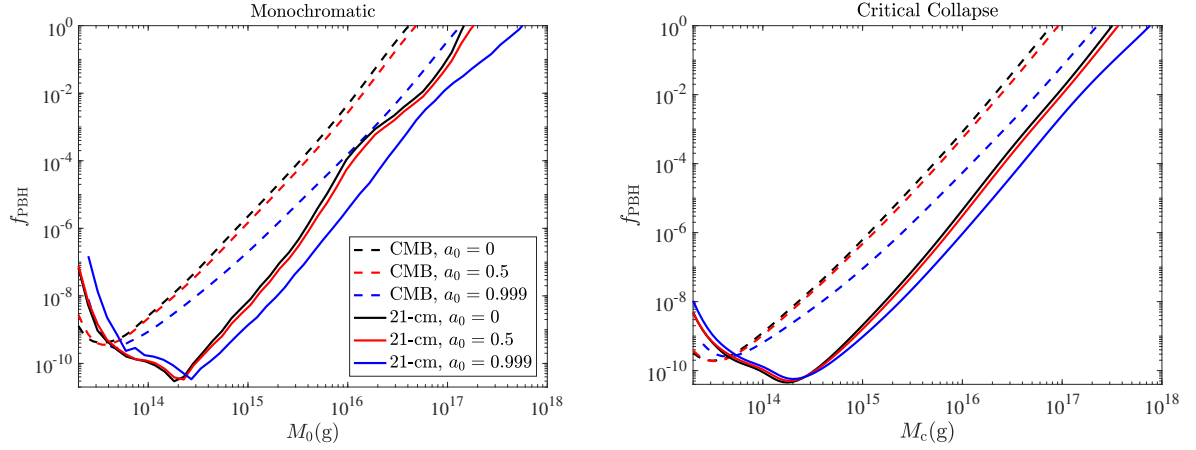


Figure 4. f_{PBH} upper bounds for monochromatic (left) and Critical Collapse (right) distributions. Constraints from 21-cm are shown in solid lines, dashed lines show marginalized 95% C.L. limits given by MCMC analysis of CMB anisotropy data from *Planck*. Black, red and blue curves show constraints for initial Kerr spin values of 0, 0.5 and 0.999 respectively. The legend applies to both panels.

T_{CMB} and T_{K} through collisional coupling and Wouthuysen-Field effect [40, 44, 102], such that at any redshifts one can expect either $T_{\text{K}} \leq T_{\text{S}} \leq T_{\text{CMB}}$ or $T_{\text{CMB}} \leq T_{\text{S}} \leq T_{\text{K}}$. Since T_{21} at $z = 17$ has been measured to be in absorption ($T_{21} < 0$) by EDGES, one can infer that at this redshift $T_{\text{K}} \leq T_{\text{S}} < T_{\text{CMB}}$, combining this with Eqs. (1.1, 4.1) and $T_{\text{CMB}} = 2.73 (1+z)$ K, we arrive at the final equation for solving our 21-cm limit on f_{PBH} ,

$$T_{\text{K}} < 49.1 \left[1 + \frac{4.14}{1 - x_{\text{e}}} \right]^{-1} \text{ K}, \quad z = 17. \quad (4.2)$$

where we have set $x_{\text{HI}} = 1 - x_{\text{e}}$ because the effect of helium reionization is negligible at this redshift [103, 104], such that $n_{\text{e}} \simeq n_{\text{p}}$ and $x_{\text{HI}} \equiv n_{\text{HI}}/(n_{\text{p}} + n_{\text{HI}}) \simeq 1 - x_{\text{e}}$.

Note that PBHs can also leave their footprints on CMB anisotropy mainly by raising the ionization level x_{e} which affects the propagation of CMB photons. On CMB temperature and polarization anisotropy spectrum, this can suppress small scale correlations and shift polarization peak locations [30]. As a comparison with 21-cm results, we also show f_{PBH} limit from the CMB. We interfaced the **CAMB** codes [105] with our modified **HyRec** for calculation of CMB anisotropy spectra in presence of Hawking radiation, and our CMB constraints on f_{PBH} are given by MCMC analysis of *Planck* 2018 data [106] using the **CosmoMC** package [107, 108]. Specifically, the datasets used are the high- ℓ plik-lite TTTEEE likelihood, low- ℓ TT and EE likelihood and the lensing likelihood. In addition to our PBH parameters, all six base Λ CDM parameters are also varied during MCMC analysis.

Figure 4 shows our 21-cm and CMB upper bounds on f_{PBH} for PBHs with monochromatic and critical collapse distributions. 21-cm constraints on the log-normal and power-law models are listed in Fig. 5 and Fig. 6. With extended mass-distributions, the number of model parameters would significantly increase the amount of computation workload. For better computational efficiency, we use a fast re-interpretation method introduced in Refs [79, 109],

$$f_{\text{PBH}}^{-1} \geq \int_{2 \times 10^{13} \text{g}}^{10^{18} \text{g}} dM_0 \frac{\Psi(M_0, t_0)}{f_{\text{max}}(M_0)}, \quad (4.3)$$

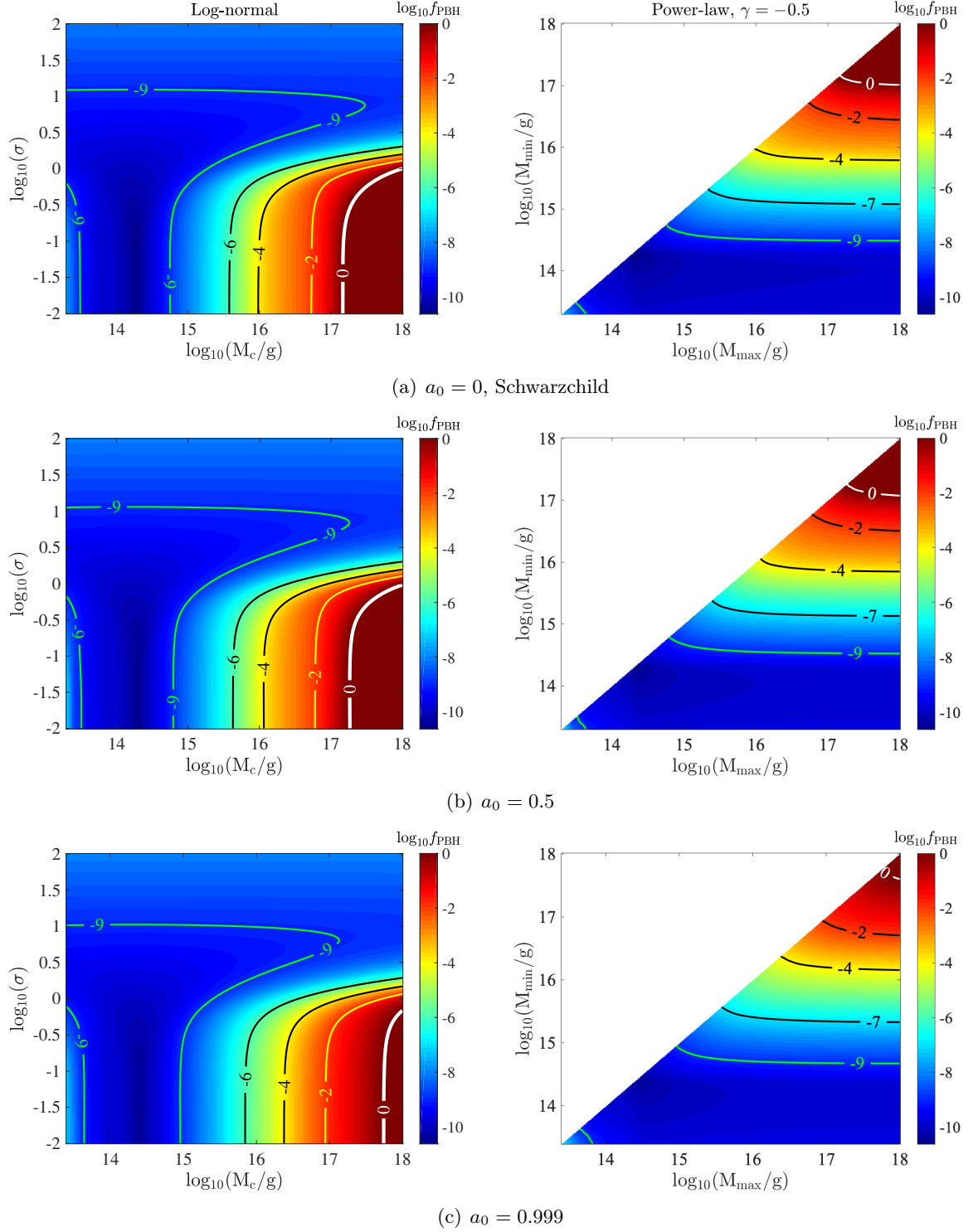
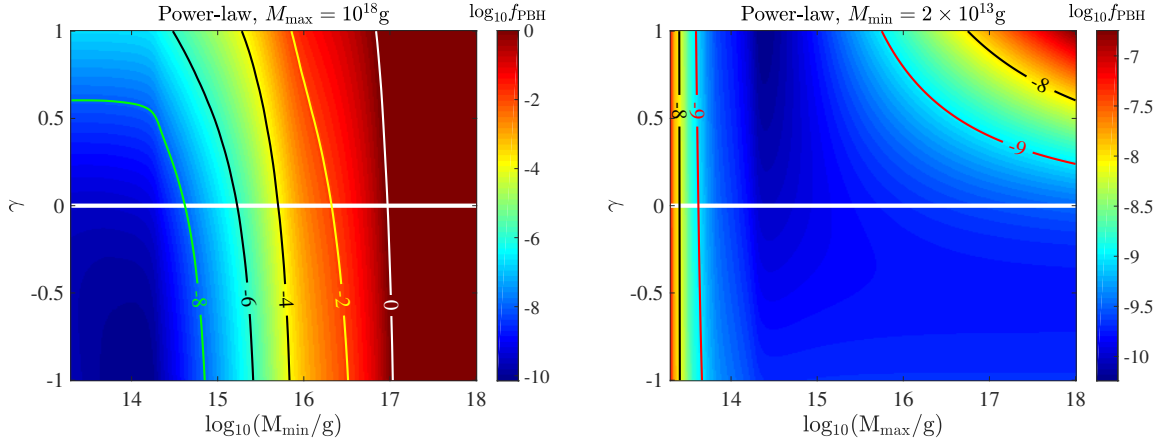
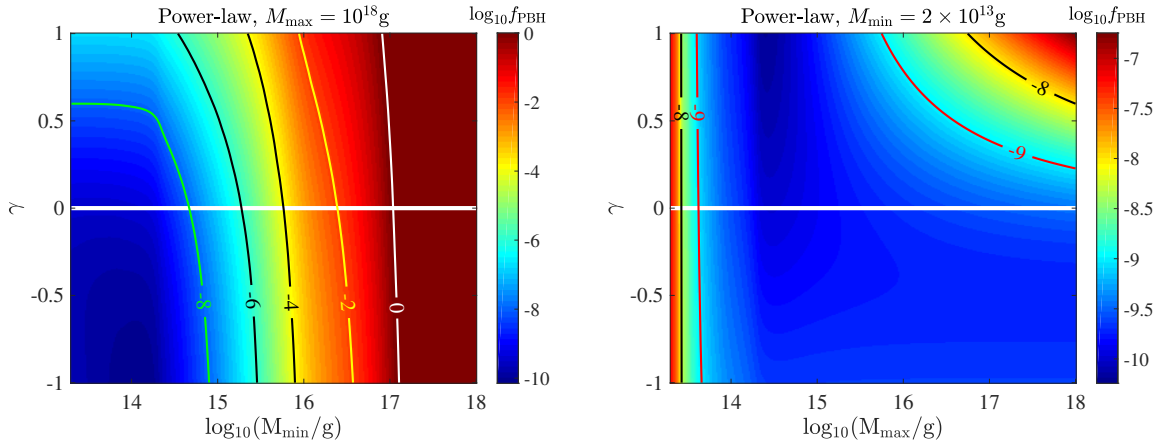


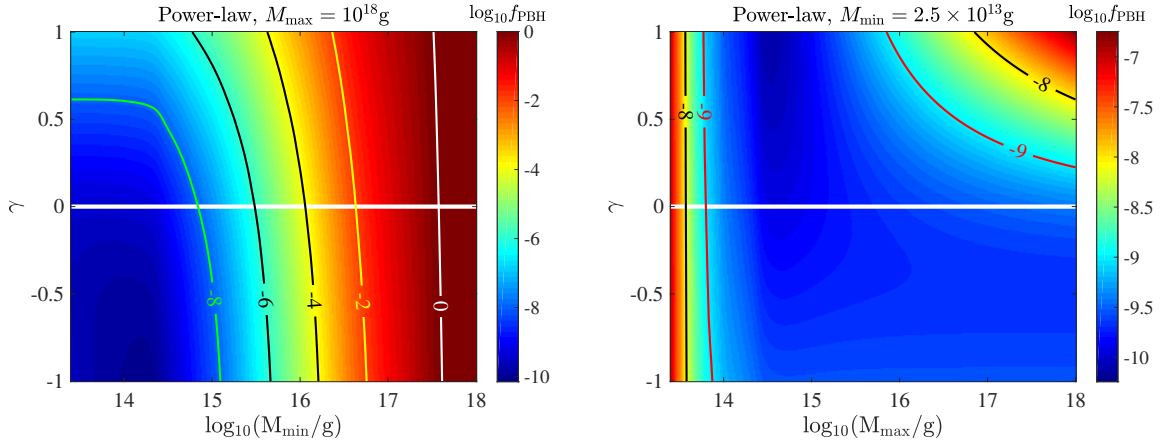
Figure 5. 21-cm upper bounds on f_{PBH} for log-normal model (left) and a power-law (right) distribution with $\gamma = -0.5$, corresponding to PBHs formed in radiation dominated epoch. The top, middle and bottom panels correspond to initial spins of $a_0 = 0, 0.5$ and 0.999 respectively. White contours show regions in which PBH can account for all DM ($f_{\text{PBH}} = 1$).



(a) $a_0 = 0$, Schwarzschild



(b) $a_0 = 0.5$



(c) $a_0 = 0.999$

Figure 6. 21-cm upper bounds on f_{PBH} for power-law distributions with fixed M_{max} (left) and M_{min} (right). The top, middle and bottom panels correspond to initial spins of $a_0 = 0$, 0.5 and 0.999 respectively. The white horizontal lines indicate power-law index $\gamma = 0$, corresponding to PBH formation in matter dominated era and is not considered here. White contours show regions in which PBH can account for all DM ($f_{\text{PBH}} = 1$).

where $f_{\text{max}}(M_0)$ is the f_{PBH} upper bounds on PBHs monochromatically distributed at M_0 . In Ref. [79] it was analytically proven that Eq. (4.3) is valid for f_{max} derived from fitting only one observable, such as solely comparing T_K at redshift $z = 17$ in our 21-cm constraints. For extended PBH distribution with multiple model parameters, Eq. (4.3) is significantly faster than iteratively solving Eq. (4.2), allowing us to compute f_{PBH} constraints for a high-resolution grid in the parameter space.

For all 21-cm constraints shown in this work, we have crosschecked that results of Eq. (4.2) and Eq. (4.3) show almost identical agreement. We also compared CMB constraints given by MCMC and Eq. (4.3) for two extended distribution scenarios: the critical collapse model and a log-normal distribution with $\sigma = 1$. Unlike the 21-cm bound, we find that Eq. (4.3) does not always apply for the CMB limit. For $M_c < 10^{15}$ g, where the evolution of PBH mass distribution cannot be ignored, Eq. (4.3) tends to overestimate f_{PBH} upper bounds, although it agrees with CosmoMC results for $M_c \geq 10^{15}$ g.

As can be seen from Fig. (4), f_{PBH} constraints set by Eq. (4.2) are more stringent than CMB by more than 2 orders of magnitude. Spinning PBHs are typically more active than Schwarzschild ones, therefore our constraint tightens for PBHs with higher spin. For the conventional monochromatic model, 21-cm excludes Schwarzschild PBHs with initial mass smaller than 1.5×10^{17} g as the dominant DM component, whereas extreme Kerr PBHs with initial spin of $a_0 = 0.999$ are ruled out for initial masses below 6×10^{17} g. 21-cm bounds become weaker than CMB for masses below 5×10^{13} g, because it is only sensitive to ionization and gas temperature at redshift 17, by which time these PBHs would have all vanished, whereas CMB can probe energy injection across much higher redshifts [96, 110].

A monochromatic distribution at M_0 can be described by a log-normal distribution with $M_c = M_0$ and $\sigma \rightarrow 0$ or a power-law distribution with $M_{\text{min}} \rightarrow M_{\text{max}} = M_0$. Under these limits, we find that bounds on log-normal and power-law distributions mimic the monochromatic constraints as expected. The critical collapse distribution is very narrow and can be fitted by a sharp log-normal distribution with $\sigma = 0.26$ [31, 79], therefore from the right panel of Fig. 4, one can see that bounds on this distribution is very similar to that on the monochromatic model. As shown in the left panels of Fig. 5, 21-cm rules out log-normal parameter space roughly confined by $[M_c < 1.5 \times 10^{17} \text{ g}, \sigma > 1]$ for $a_0 = 0$ or $[M_c < 6 \times 10^{17} \text{ g}, \sigma > 0.65]$ for $a_0 = 0.999$. The right panels of Fig. 5 illustrate 21-cm constraints on power-law distribution for PBHs formed during radiation dominated epoch ($\gamma = -0.5$), for which we find that the only allowed parameter space lies roughly at $M_{\text{min}} > 1.5 \times 10^{17}$ g for $a_0 = 0$ and $M_{\text{min}} > 6 \times 10^{17}$ g for $a_0 = 0.999$. For very wide mass distributions, which can correspond to log-normal models with $\sigma \gg 10^2$ or power-law distributions with $M_{\text{max}} \gg 10^{18}$ g, the majority of PBH density will spread outside our $[2 \times 10^{13}, 10^{18}]$ g mass window and cannot be efficiently probed by 21-cm or CMB, therefore our constraints would relax for these extreme distribution scenarios.

5 Summary

Energy injection from evaporating primordial black holes can heat up and ionize the intergalactic medium. Accumulated energy deposit into IGM gas leads to a potentially higher gas temperature near the early reionization epoch. These effects damp the amplitude of 21-cm brightness temperature T_{21} . Here we studied the 21-cm constraints on the abundance of both Schwarzschild and Kerr PBHs in $[2 \times 10^{13}, 10^{18}]$ g mass window that covers four orders of magnitudes. Mass and spin evolutions due to evaporation are accounted for, esp.

at relatively low PBH mass and high spin, that leads a non-trivial radiation energy deposit history. We considered four characteristic PBH mass distributions, in which PBHs lighter than 10^{15} grams typically lose a significant fraction of their masses by violent evaporation, or vanish entirely before the current age of the Universe. The corresponding impact on IGM gas temperature and ionization evolution are numerically computed and give stringent limits on the PBH abundance and mass distribution by comparing with current T_{21} observation data.

EDGES measures T_{21} at redshift $z = 17$ to be -500^{+200}_{-500} mK, we place our 21-cm constraints by imposing that PBH does not raise T_{21} at this redshift above -150 mK ($>99\%$ C.L.). Our results show that the global 21-cm measurement provides the currently most stringent PBH constraints across our mass window. Bounds from CMB are weaker than 21-cm by about two orders of magnitudes. Both 21-cm and CMB limits on spinning Kerr PBHs are generally tighter than Schwarzschild ones by up to two orders of magnitudes. For the conventional monochromatic mass distribution, 21-cm excludes Schwarzschild PBHs with initial mass below 1.5×10^{17} g, extreme Kerr PBHs with reduced initial spin $a_0 = 0.999$ are ruled out as the dominant DM component for masses lower than 6×10^{17} g.

For convenience with analysis, our PBH mass and abundance limits are presented for fixed initial black hole spins. It is likely for PBHs to have an extended initial spin distribution, and the corresponding limits can be derived by binning the initial spin and summing up their total heating contributions. Our PBH evolution and energy injection mainly accounts for Hawking radiation and does not include effects from black hole merger or accretion radiation. While accretion is typically small for the low PBH mass range, mergers in principle let the PBHs grow in size, slows down their evaporation and could relax the limits from energy injection. Our PBH correction to gas temperature is computed based on a otherwise standard temperature evolution in Λ CDM cosmology, and does not include any non-standard gas cooling effects that might be hinted by the magnitude of EDGES T_{21} measurement. Such effects compete with radiational heating and can be studied if confirmed by future 21-cm observations.

Acknowledgements The authors thank J. Auffinger for helpful discussions of the low-energy secondary spectrum treatment in **BlackHawk** v2. J.C and Y.G. are supported by the Ministry of Science and Technology of China under the grant number 2020YFC2201601. Y.Z.M. is supported by National Research Foundation of South Africa through grant no. 120378, 120385 and UKZN “Big Data with Science and Society” Research Flagship Project.

References

- [1] S. Hawking, *Gravitationally collapsed objects of very low mass*, *Mon. Not. Roy. Astron. Soc.* **152** (1971) 75.
- [2] B.J. Carr, *The Primordial black hole mass spectrum*, *Astrophys. J.* **201** (1975) 1.
- [3] V. Canuto, *On the origin of Hawking mini black-holes and the cold early Universe.*, *Mon. Not. Roy. Astron. Soc.* **184** (1978) 721.
- [4] M.Y. Khlopov, *Primordial Black Holes*, *Res. Astron. Astrophys.* **10** (2010) 495 [0801.0116].
- [5] B. Carr, F. Kuhnel and M. Sandstad, *Primordial Black Holes as Dark Matter*, *Phys. Rev. D* **94** (2016) 083504 [1607.06077].
- [6] A. Kashlinsky et al., *Electromagnetic probes of primordial black holes as dark matter*, **1903.04424**.

- [7] B. Carr and F. Kuhnel, *Primordial Black Holes as Dark Matter: Recent Developments*, *Ann. Rev. Nucl. Part. Sci.* **70** (2020) 355 [2006.02838].
- [8] B. Carr, K. Kohri, Y. Sendouda and J. Yokoyama, *Constraints on Primordial Black Holes*, *2002.12778*.
- [9] B. Dasgupta, R. Laha and A. Ray, *Neutrino and positron constraints on spinning primordial black hole dark matter*, *Phys. Rev. Lett.* **125** (2020) 101101 [1912.01014].
- [10] R. Laha, P. Lu and V. Takhistov, *Gas heating from spinning and non-spinning evaporating primordial black holes*, *Phys. Lett. B* **820** (2021) 136459 [2009.11837].
- [11] A. Ray, R. Laha, J.B. Muñoz and R. Caputo, *Near future MeV telescopes can discover asteroid-mass primordial black hole dark matter*, *Phys. Rev. D* **104** (2021) 023516 [2102.06714].
- [12] B. Carr, F. Kuhnel and L. Visinelli, *Constraints on Stupendously Large Black Holes*, *Mon. Not. Roy. Astron. Soc.* **501** (2021) 2029 [2008.08077].
- [13] R. Laha, *Primordial Black Holes as a Dark Matter Candidate Are Severely Constrained by the Galactic Center 511 keV γ -Ray Line*, *Phys. Rev. Lett.* **123** (2019) 251101 [1906.09994].
- [14] R. Laha, J.B. Muñoz and T.R. Slatyer, *INTEGRAL constraints on primordial black holes and particle dark matter*, *Phys. Rev. D* **101** (2020) 123514 [2004.00627].
- [15] S. Wang, D.-M. Xia, X. Zhang, S. Zhou and Z. Chang, *Constraining primordial black holes as dark matter at JUNO*, *Phys. Rev. D* **103** (2021) 043010 [2010.16053].
- [16] S. Mittal, A. Ray, G. Kulkarni and B. Dasgupta, *Constraining primordial black holes as dark matter using the global 21-cm signal with X-ray heating and excess radio background*, *2107.02190*.
- [17] O. Mena, S. Palomares-Ruiz, P. Villanueva-Domingo and S.J. Witte, *Constraining the primordial black hole abundance with 21-cm cosmology*, *Phys. Rev. D* **100** (2019) 043540 [1906.07735].
- [18] P. Villanueva-Domingo and K. Ichiki, *21 cm Forest Constraints on Primordial Black Holes*, *2104.10695*.
- [19] A. Hektor, G. Hütsi, L. Marzola, M. Raidal, V. Vaskonen and H. Veermäe, *Constraining Primordial Black Holes with the EDGES 21-cm Absorption Signal*, *Phys. Rev. D* **98** (2018) 023503 [1803.09697].
- [20] A. Halder and S. Banerjee, *Bounds on abundance of primordial black hole and dark matter from EDGES 21-cm signal*, *Phys. Rev. D* **103** (2021) 063044 [2102.00959].
- [21] A. Halder and M. Pandey, *Investigating the Effect of PBH, Dark Matter – Baryon and Dark Matter – Dark Energy Interaction on EDGES in 21cm Signal*, *2101.05228*.
- [22] A. Halder, M. Pandey, D. Majumdar and R. Basu, *Exploring multimessenger signals from heavy dark matter decay with EDGES 21-cm result and IceCube*, *2105.14356*.
- [23] Y. Yang, *The abundance of primordial black holes from the global 21cm signal and extragalactic gamma-ray background*, *Eur. Phys. J. Plus* **135** (2020) 690 [2008.11859].
- [24] Z.-C. Chen, C. Yuan and Q.-G. Huang, *Pulsar Timing Array Constraints on Primordial Black Holes with NANOGrav 11-Year Dataset*, *Phys. Rev. Lett.* **124** (2020) 251101 [1910.12239].
- [25] K. Griest, A.M. Cieplak and M.J. Lehner, *New Limits on Primordial Black Hole Dark Matter from an Analysis of Kepler Source Microlensing Data*, *Phys. Rev. Lett.* **111** (2013) 181302.
- [26] Y. Ali-Haïmoud and M. Kamionkowski, *Cosmic microwave background limits on accreting primordial black holes*, *Phys. Rev. D* **95** (2017) 043534 [1612.05644].

- [27] H. Tashiro and N. Sugiyama, *The effect of primordial black holes on 21 cm fluctuations*, *Mon. Not. Roy. Astron. Soc.* **435** (2013) 3001 [[1207.6405](#)].
- [28] Y. Yang, *Constraints on accreting primordial black holes with the global 21-cm signal*, *Phys. Rev. D* **104** (2021) 063528 [[2108.11130](#)].
- [29] Y. Yang, *Influences of accreting primordial black holes on the global 21 cm signal in the dark ages*, *Mon. Not. Roy. Astron. Soc.* **508** (2021) 5709 [[2110.06447](#)].
- [30] N. Padmanabhan and D.P. Finkbeiner, *Detecting dark matter annihilation with CMB polarization: Signatures and experimental prospects*, *Phys. Rev. D* **72** (2005) 023508 [[astro-ph/0503486](#)].
- [31] J. Cang, Y. Gao and Y. Ma, *Prospects of Future CMB Anisotropy Probes for Primordial Black Holes*, *JCAP* **05** (2021) 051 [[2011.12244](#)].
- [32] H. Poulter, Y. Ali-Haïmoud, J. Hamann, M. White and A.G. Williams, *CMB constraints on ultra-light primordial black holes with extended mass distributions*, [1907.06485](#).
- [33] P. Stöcker, M. Krämer, J. Lesgourgues and V. Poulin, *Exotic energy injection with ExoCLASS: Application to the Higgs portal model and evaporating black holes*, *JCAP* **03** (2018) 018 [[1801.01871](#)].
- [34] S.K. Acharya and R. Khatri, *CMB and BBN constraints on evaporating primordial black holes revisited*, *JCAP* **06** (2020) 018 [[2002.00898](#)].
- [35] S. Clark, B. Dutta, Y. Gao, L.E. Strigari and S. Watson, *Planck Constraint on Relic Primordial Black Holes*, *Phys. Rev. D* **95** (2017) 083006 [[1612.07738](#)].
- [36] V. Poulin, J. Lesgourgues and P.D. Serpico, *Cosmological constraints on exotic injection of electromagnetic energy*, *JCAP* **03** (2017) 043 [[1610.10051](#)].
- [37] K.J. Mack and D.H. Wesley, *Primordial black holes in the Dark Ages: Observational prospects for future 21cm surveys*, [0805.1531](#).
- [38] S. Clark, B. Dutta, Y. Gao, Y.-Z. Ma and L.E. Strigari, *21 cm limits on decaying dark matter and primordial black holes*, *Phys. Rev. D* **98** (2018) 043006 [[1803.09390](#)].
- [39] Y. Yang, *Constraints on primordial black holes and curvature perturbations from the global 21-cm signal*, *Phys. Rev. D* **102** (2020) 083538 [[2009.11547](#)].
- [40] J.R. Pritchard and A. Loeb, *21-cm cosmology*, *Rept. Prog. Phys.* **75** (2012) 086901 [[1109.6012](#)].
- [41] A. Mesinger, S. Furlanetto and R. Cen, *21cmFAST: A Fast, Semi-Numerical Simulation of the High-Redshift 21-cm Signal*, *Mon. Not. Roy. Astron. Soc.* **411** (2011) 955 [[1003.3878](#)].
- [42] M. Kuhlen, P. Madau and R. Montgomery, *The spin temperature and 21cm brightness of the intergalactic medium in the pre-reionization era*, *Astrophys. J. Lett.* **637** (2006) L1 [[astro-ph/0510814](#)].
- [43] B. Ciardi and P. Madau, *Probing beyond the epoch of hydrogen reionization with 21 centimeter radiation*, *Astrophys. J.* **596** (2003) 1 [[astro-ph/0303249](#)].
- [44] G.B. Field, *Excitation of the Hydrogen 21-CM Line*, *Proceedings of the IRE* **46** (1958) 240.
- [45] J.D. Bowman, A.E.E. Rogers, R.A. Monsalve, T.J. Mozdzen and N. Mahesh, *An absorption profile centred at 78 megahertz in the sky-averaged spectrum*, *Nature* **555** (2018) 67 [[1810.05912](#)].
- [46] A. Cohen, A. Fialkov, R. Barkana and M. Lotem, *Charting the Parameter Space of the Global 21-cm Signal*, *Mon. Not. Roy. Astron. Soc.* **472** (2017) 1915 [[1609.02312](#)].
- [47] C. Feng and G. Holder, *Enhanced global signal of neutral hydrogen due to excess radiation at cosmic dawn*, *Astrophys. J. Lett.* **858** (2018) L17 [[1802.07432](#)].

- [48] A. Ewall-Wice, T.C. Chang, J. Lazio, O. Dore, M. Seiffert and R.A. Monsalve, *Modeling the Radio Background from the First Black Holes at Cosmic Dawn: Implications for the 21 cm Absorption Amplitude*, *Astrophys. J.* **868** (2018) 63 [[1803.01815](#)].
- [49] A. Ewall-Wice, T.-C. Chang and T.J.W. Lazio, *The Radio Scream from black holes at Cosmic Dawn: a semi-analytic model for the impact of radio-loud black holes on the 21 cm global signal*, *Mon. Not. Roy. Astron. Soc.* **492** (2020) 6086 [[1903.06788](#)].
- [50] R. Jana, B.B. Nath and P.L. Biermann, *Radio background and IGM heating due to Pop III supernova explosions*, *Mon. Not. Roy. Astron. Soc.* **483** (2019) 5329 [[1812.07404](#)].
- [51] A. Fialkov and R. Barkana, *Signature of Excess Radio Background in the 21-cm Global Signal and Power Spectrum*, *Mon. Not. Roy. Astron. Soc.* **486** (2019) 1763 [[1902.02438](#)].
- [52] H. Tashiro, K. Kadota and J. Silk, *Effects of dark matter-baryon scattering on redshifted 21 cm signals*, *Phys. Rev. D* **90** (2014) 083522 [[1408.2571](#)].
- [53] J.B. Muñoz, E.D. Kovetz and Y. Ali-Haïmoud, *Heating of Baryons due to Scattering with Dark Matter During the Dark Ages*, *Phys. Rev. D* **92** (2015) 083528 [[1509.00029](#)].
- [54] R. Barkana, *Possible interaction between baryons and dark-matter particles revealed by the first stars*, *Nature* **555** (2018) 71 [[1803.06698](#)].
- [55] J.R. Bhatt, P.K. Natwariya, A.C. Nayak and A.K. Pandey, *Baryon-Dark matter interaction in presence of magnetic fields in light of EDGES signal*, *Eur. Phys. J. C* **80** (2020) 334 [[1905.13486](#)].
- [56] P.K. Natwariya, A.C. Nayak and T. Srivastava, *Constraining Spinning Primordial Black Holes With Global 21 cm Signal*, [2107.12358](#).
- [57] T. Chiba and S. Yokoyama, *Spin Distribution of Primordial Black Holes*, *PTEP* **2017** (2017) 083E01 [[1704.06573](#)].
- [58] M. Mirbabayi, A. Gruzinov and J. Noreña, *Spin of Primordial Black Holes*, *JCAP* **03** (2020) 017 [[1901.05963](#)].
- [59] V. De Luca, V. Desjacques, G. Franciolini, A. Malhotra and A. Riotto, *The initial spin probability distribution of primordial black holes*, *JCAP* **05** (2019) 018 [[1903.01179](#)].
- [60] M.Y. Khlopov and A.G. Polnarev, *Primordial black holes as a cosmological test of grand unification*, *Phys. Lett. B* **97** (1980) 383.
- [61] T. Harada, C.-M. Yoo, K. Kohri and K.-I. Nakao, *Spins of primordial black holes formed in the matter-dominated phase of the Universe*, *Phys. Rev. D* **96** (2017) 083517 [[1707.03595](#)].
- [62] E. Cotner, A. Kusenko and V. Takhistov, *Primordial Black Holes from Inflaton Fragmentation into Oscillons*, *Phys. Rev. D* **98** (2018) 083513 [[1801.03321](#)].
- [63] T. Kokubu, K. Kyutoku, K. Kohri and T. Harada, *Effect of Inhomogeneity on Primordial Black Hole Formation in the Matter Dominated Era*, *Phys. Rev. D* **98** (2018) 123024 [[1810.03490](#)].
- [64] M. He and T. Suyama, *Formation threshold of rotating primordial black holes*, *Phys. Rev. D* **100** (2019) 063520 [[1906.10987](#)].
- [65] Y. Bai and N. Orlofsky, *Primordial Extremal Black Holes as Dark Matter*, *Phys. Rev. D* **101** (2020) 055006 [[1906.04858](#)].
- [66] E. Cotner, A. Kusenko, M. Sasaki and V. Takhistov, *Analytic Description of Primordial Black Hole Formation from Scalar Field Fragmentation*, *JCAP* **10** (2019) 077 [[1907.10613](#)].
- [67] A. Arbey, J. Auffinger and J. Silk, *Evolution of primordial black hole spin due to Hawking radiation*, *Mon. Not. Roy. Astron. Soc.* **494** (2020) 1257 [[1906.04196](#)].

- [68] M.M. Flores and A. Kusenko, *Spins of primordial black holes formed in different cosmological scenarios*, [2106.03237](#).
- [69] J.H. MacGibbon and B.R. Webber, *Quark and gluon jet emission from primordial black holes: The instantaneous spectra*, *Phys. Rev. D* **41** (1990) 3052.
- [70] PLANCK collaboration, *Planck 2018 results. VI. Cosmological parameters*, *Astron. Astrophys.* **641** (2020) A6 [[1807.06209](#)].
- [71] D.N. Page, *Particle emission rates from a black hole: Massless particles from an uncharged, nonrotating hole*, *Phys. Rev. D* **13** (1976) 198.
- [72] D.N. Page, *Particle emission rates from a black hole. ii. massless particles from a rotating hole*, *Phys. Rev. D* **14** (1976) 3260.
- [73] A. Arbey and J. Auffinger, *BlackHawk: A public code for calculating the Hawking evaporation spectra of any black hole distribution*, *Eur. Phys. J. C* **79** (2019) 693 [[1905.04268](#)].
- [74] A. Arbey and J. Auffinger, *Physics Beyond the Standard Model with BlackHawk v2.0*, [2108.02737](#).
- [75] S.W. Hawking, *Particle Creation by Black Holes*, *Commun. Math. Phys.* **43** (1975) 199.
- [76] R. Dong, W.H. Kinney and D. Stojkovic, *Gravitational wave production by Hawking radiation from rotating primordial black holes*, *JCAP* **10** (2016) 034 [[1511.05642](#)].
- [77] J.H. MacGibbon, *Quark and gluon jet emission from primordial black holes. 2. The Lifetime emission*, *Phys. Rev. D* **44** (1991) 376.
- [78] A. Dolgov and J. Silk, *Baryon isocurvature fluctuations at small scales and baryonic dark matter*, *Phys. Rev. D* **47** (1993) 4244.
- [79] B. Carr, M. Raidal, T. Tenkanen, V. Vaskonen and H. Veermäe, *Primordial black hole constraints for extended mass functions*, *Phys. Rev. D* **96** (2017) 023514 [[1705.05567](#)].
- [80] A.M. Green, *Microlensing and dynamical constraints on primordial black hole dark matter with an extended mass function*, *Phys. Rev. D* **94** (2016) 063530 [[1609.01143](#)].
- [81] J. Yokoyama, *Cosmological constraints on primordial black holes produced in the near critical gravitational collapse*, *Phys. Rev. D* **58** (1998) 107502 [[gr-qc/9804041](#)].
- [82] J.C. Niemeyer and K. Jedamzik, *Dynamics of primordial black hole formation*, *Phys. Rev. D* **59** (1999) 124013 [[astro-ph/9901292](#)].
- [83] N. Bellomo, J.L. Bernal, A. Raccanelli and L. Verde, *Primordial Black Holes as Dark Matter: Converting Constraints from Monochromatic to Extended Mass Distributions*, *JCAP* **01** (2018) 004 [[1709.07467](#)].
- [84] S. Pi, Y.-l. Zhang, Q.-G. Huang and M. Sasaki, *Scalaron from R^2 -gravity as a heavy field*, *JCAP* **05** (2018) 042 [[1712.09896](#)].
- [85] B. Carr, T. Tenkanen and V. Vaskonen, *Primordial black holes from inflaton and spectator field perturbations in a matter-dominated era*, *Phys. Rev. D* **96** (2017) 063507 [[1706.03746](#)].
- [86] M. Fishbach, D.E. Holz and B. Farr, *Are LIGO's Black Holes Made From Smaller Black Holes?*, *Astrophys. J. Lett.* **840** (2017) L24 [[1703.06869](#)].
- [87] Z. Doctor, B. Farr and D.E. Holz, *Black Hole Leftovers: The Remnant Population from Binary Black Hole Mergers*, *Astrophys. J. Lett.* **914** (2021) L18 [[2103.04001](#)].
- [88] S. Fakhry, J.T. Firouzjaee and M. Farhoudi, *Primordial Black Hole Merger Rate in Ellipsoidal-Collapse Dark Matter Halo Models*, *Phys. Rev. D* **103** (2021) 123014 [[2012.03211](#)].
- [89] S. Fakhry, M. Naseri, J.T. Firouzjaee and M. Farhoudi, *Primordial Black Hole Merger Rate in Self-Interacting Dark Matter Halo Models*, [2106.06265](#).

- [90] D. Ł. Król and A. Janiuk, *Accretion-induced Black Hole Spin-up Revised by Numerical General Relativistic MHD*, *Astrophys. J.* **912** (2021) 132 [[2104.00741](#)].
- [91] P.E. Nelson, Z.B. Etienne, S.T. McWilliams and V. Nguyen, *Induced Spins from Scattering Experiments of Initially Nonspinning Black Holes*, *Phys. Rev. D* **100** (2019) 124045 [[1909.08621](#)].
- [92] S. Jaraba and J. Garcia-Bellido, *Black hole induced spins from hyperbolic encounters in dense clusters*, [2106.01436](#).
- [93] T. Harada, C.-M. Yoo, K. Kohri, K.-i. Nakao and S. Jhingan, *Primordial black hole formation in the matter-dominated phase of the Universe*, *Astrophys. J.* **833** (2016) 61 [[1609.01588](#)].
- [94] T.R. Slatyer and C.-L. Wu, *General Constraints on Dark Matter Decay from the Cosmic Microwave Background*, *Phys. Rev. D* **95** (2017) 023010 [[1610.06933](#)].
- [95] H. Liu, T.R. Slatyer and J. Zavala, *Contributions to cosmic reionization from dark matter annihilation and decay*, *Phys. Rev. D* **94** (2016) 063507 [[1604.02457](#)].
- [96] J. Cang, Y. Gao and Y.-Z. Ma, *Probing dark matter with future CMB measurements*, *Phys. Rev. D* **102** (2020) 103005 [[2002.03380](#)].
- [97] Y. Ali-Haïmoud and C.M. Hirata, *HyRec: A fast and highly accurate primordial hydrogen and helium recombination code*, *Phys. Rev. D* **83** (2011) 043513 [[1011.3758](#)].
- [98] S. Seager, D.D. Sasselov and D. Scott, *A new calculation of the recombination epoch*, *Astrophys. J. Lett.* **523** (1999) L1 [[astro-ph/9909275](#)].
- [99] T.R. Slatyer, *Indirect Dark Matter Signatures in the Cosmic Dark Ages II. Ionization, Heating and Photon Production from Arbitrary Energy Injections*, *Phys. Rev. D* **93** (2016) 023521 [[1506.03812](#)].
- [100] T.R. Slatyer, *Energy Injection And Absorption In The Cosmic Dark Ages*, *Phys. Rev. D* **87** (2013) 123513 [[1211.0283](#)].
- [101] K. Cheung, J.-L. Kuo, K.-W. Ng and Y.-L.S. Tsai, *The impact of EDGES 21-cm data on dark matter interactions*, *Phys. Lett. B* **789** (2019) 137 [[1803.09398](#)].
- [102] S. Mittal and G. Kulkarni, *Ly α coupling and heating at cosmic dawn*, *Mon. Not. Roy. Astron. Soc.* **503** (2021) 4264 [[2009.10746](#)].
- [103] E. Puchwein, F. Haardt, M.G. Haehnelt and P. Madau, *Consistent modelling of the meta-galactic UV background and the thermal/ionization history of the intergalactic medium*, *Mon. Not. Roy. Astron. Soc.* **485** (2019) 47 [[1801.04931](#)].
- [104] A. Sokasian, T. Abel and L.E. Hernquist, *The epoch of helium reionization*, *Mon. Not. Roy. Astron. Soc.* **332** (2002) 601 [[astro-ph/0112297](#)].
- [105] A. Lewis, A. Challinor and A. Lasenby, *Efficient computation of CMB anisotropies in closed FRW models*, *Astrophys. J.* **538** (2000) 473 [[astro-ph/9911177](#)].
- [106] PLANCK collaboration, *Planck 2018 results. V. CMB power spectra and likelihoods*, *Astron. Astrophys.* **641** (2020) A5 [[1907.12875](#)].
- [107] A. Lewis and S. Bridle, *Cosmological parameters from CMB and other data: A Monte Carlo approach*, *Phys. Rev. D* **66** (2002) 103511 [[astro-ph/0205436](#)].
- [108] A. Lewis, *Efficient sampling of fast and slow cosmological parameters*, *Phys. Rev. D* **87** (2013) 103529 [[1304.4473](#)].
- [109] F. Kühnel and K. Freese, *Constraints on Primordial Black Holes with Extended Mass Functions*, *Phys. Rev. D* **95** (2017) 083508 [[1701.07223](#)].
- [110] D.P. Finkbeiner, S. Galli, T. Lin and T.R. Slatyer, *Searching for dark matter in the cmb: A compact parametrization of energy injection from new physics*, *Phys. Rev. D* **85** (2012) 043522.